Journal of New Materials for Electrochemical Systems 12, 177-185 (2009)

Characterization of Nb and W Doped Titania as Catalyst Supports for Proton Exchange Membrane Fuel Cells

H. Chhina[*,1,2], S. Campbell[1] and O. Kesler[2]

[1]AFCC-Automotive Fuel Cell Cooperation Corp., 9000 Glenlyon Parkway, Burnaby, BC, Canada V5J 5J8
[2]Department of Mechanical and Industrial Engineering, 5 King's College Road, University of Toronto, Toronto, Ontario, Canada, M5S 3G8

Received: January 29, 2009, Accepted: September 24, 2009

Abstract: *Niobium doped titania and tungsten doped titania prepared using a sol-gel technique were evaluated as possible catalyst support materials for proton exchange membrane fuel cells. The electrical conductivity of the doped materials prepared under different heat-treatment temperatures and partial oxygen pressures was measured. Rutile 10Nb-TiO_2 was extremely conductive compared to the anatase 10Nb-TiO_2. For the W doped samples the conductivity was found to be extremely low compared to the rutile 10Nb-TiO_2, and W segregation was observed when the material was reduced in H_2 at temperatures greater than 700°C. X-ray photoelectron spectroscopy (XPS) analysis was completed on 10Nb-TiO_2 calcined at 500°C and on 10Nb-TiO_2 calcined and then reduced at a range of temperatures (500°C to 900°C).*

Keywords: Catalyst support, oxidation, titania, tungsten doped titania, niobium doped titania, carbon, proton exchange membrane fuel cells, electrocatalyst

1. INTRODUCTION

For automotive applications, proton exchange membrane fuel cells must endure frequent startup-shutdown cycles. During start-up, electrode potentials up to 1.5V may be experienced for short periods of time, leading to a significant degradation in the fuel cell performance due to oxidation of the carbon catalyst support [1,2]. Platinum, with its high activity for oxygen reduction, is usually supported on a high surface area carbon to achieve a high dispersion of the precious metal catalyst on an electrically conductive support. The oxidation of carbon to carbon dioxide (equation 1), however, is significant at potentials above 0.9V vs. RHE [3] and leads to loss of active Pt surface area [4], resulting in performance degradation. It is therefore critical to develop and evaluate non-carbon alternatives.

$$C+2H_2O \rightarrow CO_2+4H^++4e^- \quad (1)$$

Metal oxides are one of the most important categories of solid catalysts or catalyst supports and are widely used in heterogeneous catalysis [5]. Sub-stoichiometric or doped metal oxides based on TiO_2 are n-type semiconductors. TiO_2 is notable for its photocatalytic and strong metal support interaction (SMSI) properties [6]. Titania is also readily available, cheap, and non-toxic [7]. Niobium doped titania [8-10] and non-stoichiometric titania [10,11] have been studied as non-carbon catalyst supports.

Many binary stoichiometric oxides such as titanium dioxide (TiO_2) are resistive. The electronic conductivity of titanium-based ceramics originates from the presence of Ti^{3+} ions, which can be made by either creating oxygen vacancies by heating TiO_2 in a reducing atmosphere, or by introducing appropriate dopants, *e.g.*, niobium (Nb). Sub-stoichiometric titania (e.g. Ti_4O_7) exhibits a high electrical conductivity of 1000 Scm^{-1} at room temperature, compared to graphitized carbon with a conductivity of 727 Scm^{-1} [10]. Work by Ioroi et al. [12] showed that Pt/Ti_4O_7 is stable under fuel cell conditions, but since the support was synthesized at high temperatures, the resulting surface area was low. The drawback with non-stoichiometric titania is that under fuel cell operation, it can become stoichiometric and form a resistive layer of

*To whom correspondence should be addressed:
Email: harmeet.chhina@afcc-auto.com,
Phone: +1-604-453-3834, fax: +1-604-453-3782

TiO_2 at the three-phase reaction interface [10]. The anatase to rutile transformation in synthetic titania usually occurs between 600 and 700°C, but for some applications it is required that the anatase titania be stable at 900°C [13]. The anatase phase of titania is usually stabilized by cation addition. Addition of Cr, La, W, Mo, Fe, Pt or Nb to TiO_2 has been studied for better sensing performance [14]. Niobium addition has been found to be effective for enhancing the sensitivity and shortening the response time for TiO_2 based oxygen sensors [14]. Also, Nb addition raises the anatase to rutile transition temperature [15,15-22].

Studies have been performed on Nb-doped titania catalyst supports, but to the best of the authors' knowledge the characterization of these materials and their properties relevant to PEMFC performance prepared under different oxygen partial pressures has not previously been reported out.

Tungsten doped titania is another candidate support material that has not been studied as a novel non-carbon catalyst support. The natural abundance in the earth's crust and annual world production of tungsten are approximately 160 ppm and 45,000 tons, respectively, and those of niobium are 20 ppm and 15,000 tons, respectively [23]. Tungsten can also sustain more oxidation states (2, 3, 4, 5, and 6) than Nb (3, 4 and 5). For tungsten doped titania, it may be hypothesized that the tungsten may exist in multiple simultaneous oxidation states over a wider range of temperatures and partial oxygen pressures, which might aid in enhancing the electrical conductivity. W-TiO_2 was studied as a candidate support material along with Nb-TiO_2. Tungsten doped titania has been applied in industry for sensor applications [24], for the selective reduction of NO_x in exhaust gases [25], for self cleaning windows [26], and for photocatalysis [27]. There are no published studies on the use of W-doped titania as a potential catalyst support for PEMFCs. If a W ion substitutes a Ti ion, the valence state of some Ti atoms will be reduced to Ti^{3+} increasing the conductivity of the material [24].

The types of defects that are introduced by addition of Nb into titania depend on the conditions used to synthesize the material. If Nb is in the Nb^{5+} oxidation state, then charge compensation for Nb^{5+} substitution for Ti^{4+} is achieved either by the creation of one Ti cation vacancy per four Nb atoms introduced (equation 2), or by the stoichiometric reduction of Ti^{4+} to Ti^{3+} (equation 3) [14]. The occurrence of either of these scenarios will depend on the synthesis conditions, partial pressure of oxygen, and temperature. Oxidative conditions and low concentrations of Nb would favor generation of titanium vacancies because cations would be maintained in their higher oxidation state, whereas Ti^{4+} to Ti^{3+} reduction would predominate for reductive and high Nb concentration conditions [14].

$$Nb_2O_5 \xrightarrow{Ti_2O_4} 2Nb_{Ti}^{\cdot} + 2Ti_{Ti}' + 4O_O^X + 1/2O_{2(g)} \quad (2)$$

$$2Nb_2O_5 \xrightarrow{Ti_5O_{10}} 4Nb_{Ti}^{\cdot} + V_{Ti}'''' + 10O_O^X \quad (3)$$

Similarly to titania, Nb also forms an oxide with the rutile structure, so doping of rutile titania with Nb occurs easily [28]. Up to 30 atom% Nb can be substitutionally incorporated into the titania lattice due to the similarity between the ionic radii of Ti^{4+} and Nb^{5+} (0.61Å and 0.64Å, respectively) [29]. Nb incorporation into the titania leads to new electronic states in the titania band structure [29]. Nb doping gives rise to shallow donor states that are ~0.02-0.03 eV below the conduction band minimum, giving essentially the same energy as the donor states introduced by oxygen deficiency [30].

Park et al. [31] have prepared Nb doped titania as a catalyst support for PEMFCs by hydrothermal synthesis. The hydrothermal reaction was conducted at 120°C for 20h. In order to activate the Nb dopant, the samples were treated at 400°C for 2h under pure H_2 gas flowing at 300 sccm. 40wt%Pt was supported on Nb-TiO_2 catalyst support using the same method used to synthesize 40wt%Pt/Vulcan XC-72. The volume ratio of Pt to 10Nb-TiO_2 is high in this case compared to Pt on carbon due to the density difference between the Nb-TiO_2 support and carbon. The support produced was a mixture of anatase and rutile titania with a particle size of ~10nm. The electrical conductivity of the material was not determined. The electrocatalytic activity of the supported catalyst was determined using the oxygen reduction current. The Pt/Nb-TiO_2 electrocatalyst was reported to have higher ORR currents than Pt/Vulcan XC-72.

Koninck et al. [8] studied the use of Nb-doped titania synthesized by sol-gel methods as a conductive support for catalysts in rechargeable metal-air batteries. They studied the electrochemical behaviour of Nb-doped titania (5 at% and 10 at% Nb) as a catalyst support over a wide potential range involving water electrolysis in an alkaline medium. The sol-gel derived Nb-TiO_2 was calcined at 450°C, 650°C, or 1050°C for 2 hours in air. The XPS results showed that the samples calcined at 450°C or at 650°C had Ti^{4+} and Nb^{4+}, but the samples calcined at 1050°C had a separate TiNb$_2$O$_7$ phase for the 10 at% Nb sample.

Garcia et al. [32] synthesized 10Nb-TiO_2 support using a sol-gel technique with a templating agent as a catalyst support for direct methanol fuel cells. After the synthesis, the doped titania support was dried at 100°C for 12 hours. There were no further heat treatments applied to this material. The support material was anatase with a Brunauer Emmett Teller (BET) surface area of 136 m^2g^{-1}.

Park et al. [31] reduced the doped material directly after synthesizing, whereas Koninck et al. [8] calcined the support material and Garcia et al. [32] applied no heat treatments in order to obtain a conductive support. It has been reported in the literature that the electrical conductivity of Nb-doped titania is significantly impacted by the synthesis conditions [14]. As discussed above, the types of defects are different depending on whether oxidizing or reducing conditions are used during the synthesis. In this study, in order to examine the effects of temperature and partial oxygen pressures on the support properties, the synthesized materials have been subjected to several heat treatments and atmospheres and their resulting physical properties characterized. Various synthesis routes of mesoporous TiO_2 have been reported, including addition of surfactants as templating agents. Ideally, the surfactant removal would leave a structure with high porosity; but, unfortunately, complete surfactant removal from these structures without collapse of the framework is difficult [7], so templating was not used in this study. The effect on electrical conductivity of direct reduction versus calcination and then reduction of the doped oxides was studied. The TEM observation of Pt supported on 10Nb-TiO_2 and the fuel cell testing are reported elsewhere [33,34].

2. EXPERIMENTAL PROCEDURE

A sol-gel method was used in this study to synthesize doped titania in a similar way to studies previously reported in the litera-

ture [7,13-15,17,35-39]. Different reducing temperatures were applied to 10Nb-TiO_2, with an atmosphere of 100% H_2 flowing at 300 ml min^{-1} being used for the reduction experiments. Calcining was performed in still air. The characterization of the material included measurement of the electrical conductivity, x-ray diffraction (XRD), BET surface area measurement, scanning electron microscopy (SEM), X-ray photoelectron spectroscopy (XPS) and transmission electron microscopy (TEM).

2.1. Synthesis of 10Nb-TiO_2

A modified method of Nazar et al. [7] was used for the synthesis of 10Nb-TiO_2. Titanium propoxide [$Ti(OPr)_4$; 99.999%, Aldrich; 17.1g] was dissolved in 66g of propan-2-ol. The solution was stirred for 15 minutes followed by addition of deionized water (33g). The hydrolysis product mixture was then covered and aged for ~18h at room temperature. For the niobium (Nb) doped titania samples, niobium (V) ethoxide ($Nb(OC_2H_5)_5$, Alfa Aesar) was added to the titanium propoxide before the hydrolysis step in a mole ratio of 10mol%Nb and the rest of the procedure was the same as that for the titania synthesis mentioned above. The white precipitate was then filtered and dried at 120°C for 6 hrs. The resulting powder was then either reduced directly or first calcined at 500°C for 6 hours in a tube furnace heated at 5°C min^{-1} and then later reduced. Prior to reduction, the samples were placed in a tube furnace followed by purging of the tube with hydrogen at 950 ml min^{-1} for 30 minutes and then at 300 ml min^{-1} for another 30 minutes. The reducing conditions involved heat-treating the samples in a tube furnace at 500°C, 600°C, 700°C or 900°C for 2 hours under 300 ml min^{-1} of H_2, with a heating rate of 10°C min^{-1}. The flow rate of hydrogen was the same as that reported by Park et al. [9].

2.2. Synthesis of W-TiO_2

A similar method to that used to synthesize Nb-TiO_2, as described above, was used to synthesize 5, 10, 15 and 20 mol% W doped titania. Tungsten (V) ethoxide [Alfa Aesar] was used as the tungsten precursor. For the W doped titania materials, all the samples were directly reduced at 400, 500, or 600°C. Samples of 10W-TiO_2 and 20W-TiO_2 were also reduced at 700°C and 900°C. Separate samples of 10W-TiO_2 were also first calcined at 500°C and then reduced at 400, 500, or 600°C in order to compare the properties of first calcined and then reduced materials to those of the directly reduced material.

2.3. Characterization

2.3.1. XRD/TGA/SEM/TEM/BET/XPS

X-Ray Diffraction (XRD) was used to determine the presence of different phases of titania and the presence of crystalline Pt on the support. Crystallite sizes were calculated using the Scherrer equation [40]:

$$t = 0.9\,\lambda/(b\cos\theta_b) \quad (4)$$

where t = crystallite size in Å, λ is the wavelength (1.5406 Å in this case for Cu Kα radiation), b is the full-width at half maximum (FWHM) of a peak in the XRD spectrum, and q_b is the diffraction angle for that peak. Determination of the full width at half maximum (FWHM) is expected to dominate the measurement error, with the FWHM error estimated to be 10%.

Thermogravimetric analysis (TGA) was used to determine any weight change for the dried 10Nb-TiO_2 sample and the calcined 10Nb-TiO_2 sample after oxidation in air flowing at 40 ml min^{-1}. The temperature was ramped from room temperature to 50°C at 2°C min^{-1}. The sample was then held at 50°C for five minutes to allow time for water removal. The sample was then ramped from 50°C to 900°C at 2°C min^{-1}. The data were analyzed by plotting normalized weight for each material versus temperature.

A 200kV Hitachi H-800 transmission electron microscope (TEM) and EDX in a Scanning Electron Microscope (Philips XL30)))) were used to examine the microstructure and to verify the Nb and Ti content. BET surface area measurement of the support materials was carried out in a Nova 2000e surface area analyzer.

XPS spectra were acquired with a Thermo Scientific ThetaProbe XPS (East Grinstead, UK) using an Al Ka excitation source, with pass energies of 200 eV and 20 eV for survey and high-resolution scans, respectively. Measurements were collected in the analysis chamber at 10^{-7} mbar. The XPS was used to determine the oxidation state of niobium and titanium in the doped oxides treated under different atmospheres. Binding energies were referenced to the Ti $2p_{3/2}$ peak at 458.7 eV.

2.4. Electrical conductivity

Pellets of different materials were made in order to measure the electrical resistance. In order to add a similar volume of the samples with different densities, the density of rutile and anatase titania with 10mol%Nb doping was first calculated as:

$$\textit{Density} \qquad \rho = \Sigma n_i A_i/(V_c N_A) \quad (5)$$

where n_i = number of atoms of species i in a unit cell, A_i = atomic weight of each species in g mol^{-1}, V_c = volume of a unit cell in cm^3, and N_A is Avogadro's number (6.02×10^{23} atoms mol^{-1}). The unit cell volumes of anatase and of rutile are 136.1 and 62.4 $Å^3$, respectively [41]. Using these values, the density of the anatase phase was calculated to be 3.89 g cm^{-3} and that for the rutile phase was 4.25 g cm^{-3}, which are close to the reported values of 3.85 g cm^{-3} and 4.25 g cm^{-3}, respectively [42]. For the 10Nb-TiO_2 anatase phase the density was calculated as:

$$\rho = n\,[A_{Ti}*mol\%Ti + A_{Nb}*mol\%Nb + A_{O2}]/(V_c N_A) \quad (6)$$

$\rho = 4[(47.9*0.9) + (92.9*0.1)+32]/[136.1\times10^{-24}cm^3 * 6.02\times10^{23}$ atoms $mol^{-1}]$

Using these values, the density of anatase 10mol%Nb doped titania was calculated to be 4.12 g cm^{-3} and that for the rutile phase was calculated to be 4.49 g cm^{-3}. In the current study, if there was any change in the lattice constants observed by XRD, the measured lattice constants were used to calculate the unit cell volume and therefore the density of the cell. Similarly, the volume of the powder required for the W-TiO_2 pellets was also calculated for samples with different W amounts.

The pellets were made using a 10mm diameter die with a hydraulic uniaxial press. The powders were pressed at 0.7 GPa for 60s. Both sides of the pellets were then painted with a conductive silver paint and copper strips were mounted on both sides of the pellets using silver loaded epoxy. A DC measurement was conducted between +100 and –100mV, with the resulting current measured in order to evaluate the resistance of the pellets.

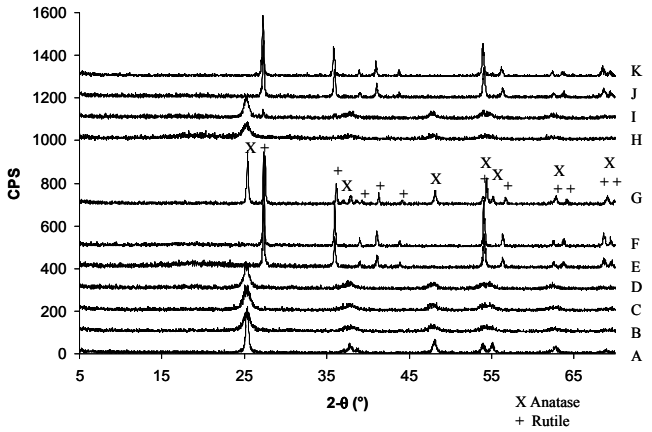

Figure 1. X-ray diffraction pattern for TiO_2 and 10Nb-TiO_2 treated under different temperatures. Samples A and B were calcined at 500°C for 6h with a 5°C min^{-1} heating rate. Samples C-K were treated in 300 sccm H_2 for 2h with a 10°C min^{-1} heating rate. A) TiO_2 calcined at 500°C, B) 10Nb-TiO_2 calcined at 500°C, C) 10Nb-TiO_2 calcined and then reduced at 500°C, D) 10Nb-TiO_2 calcined and then reduced at 600°C, E) 10Nb-TiO_2 calcined and then reduced at 700°C, F) 10Nb-TiO_2 calcined and then reduced at 900°C, G) TiO_2 reduced at 600°C, H) 10Nb-TiO_2 reduced at 500°C, I) 10Nb-TiO_2 reduced at 600°C, J) 10Nb-TiO_2 reduced at 700°C, K) 10Nb-TiO_2 reduced at 900°C.

Table 1. Crystallite size calculated from the X-ray diffraction patterns of TiO_2 and 10Nb-TiO_2 using the Scherrer equation.

		Crystal size (nm)	
		Anatase	Rutile
TiO_2	Calcined at 500ºC	20	
	Reduced at 600ºC	38	57
10Nb-TiO_2	Calcined at 500ºC	10	
	Calcined than reduced at 500ºC	10	
	Calcined than reduced at 600ºC	11	
	Calcined than reduced at 700ºC		39
	Calcined than reduced at 900ºC		56
	Reduced at 500ºC	13	
	Reduced at 600ºC	16	
	Reduced at 700ºC		39
	Reduced at 900ºC		44

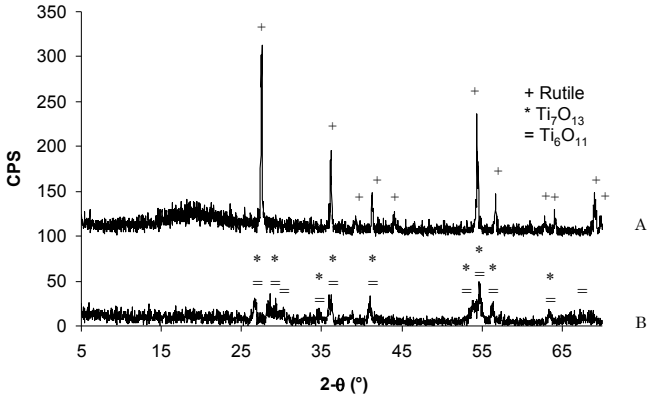

Figure 2. X-ray diffraction pattern of TiO_2 calcined and then reduced at A) 700°C, and B) 900°C.

3. RESULTS AND DISCUSSION

3.1. Characterization-TGA, XRD, BET

3.1.1. 10Nb-TiO_2

The 10Nb-TiO_2 calcined at 500°C was a white powder. As this white powder was reduced under increasing temperatures, the material was found to darken in colour. The 10Nb-TiO_2 material reduced at 500°C was a pale blue powder, and the 10Nb-TiO_2 calcined then reduced at 900°C was a dark blue powder.

Thermogravimetric analysis (TGA) was conducted on 10Nb-TiO_2 both after drying at 120°C for 6 hours and after calcination at 500°C for 6 hours. The TGA data (not shown here) showed a weight loss of approximately 12% in the dried samples, which is attributed to the loss of trapped organics and water [43]. The calcined samples had less than ~3% weight loss.

Figure 1 shows x-ray diffraction patterns for various samples that were either calcined or reduced or both under different conditions. The titania sample calcined at 500°C (Figure 1A) was anatase with a crystallite size of 20 nm (Table 1), which was calculated from the Scherrer equation using the 2q 25.2° (101) peak. The 10Nb-TiO_2 when calcined was also anatase (Figure 1B), with 10 nm-sized crystallites. When the 10Nb-TiO_2 calcined sample was later reduced at 500°C or 600°C for 2 hours, the material remained anatase with 10 nm and 11 nm-sized crystallites, respectively (Figure 1C and D). The 10Nb-TiO_2 when calcined and then reduced at 700°C or 900°C (Figure 1E and F) exhibited only the rutile phase, with crystallite sizes of 39 and 56 nm, respectively. The dominant rutile peak at 2q 27.4° (110) was used to calculate the rutile crystallite size. Figure 1 G-K show the diffraction patterns for materials that were directly reduced. In contrast with the doped titania, the undoped TiO_2 when reduced at 600°C (Figure 1G) produced a mixture of anatase and rutile titania with 38 nm sized anatase crystallites and 57 nm sized rutile crystallites. For the samples that were directly reduced, pure anatase phase was observed for the sample reduced at 500°C (Figure 1H), with an average crystallite size of 13 nm. Unlike the sample calcined and then reduced at 600°C, the sample directly reduced at 600°C (Figure 1I) had a mixture of both anatase and rutile phase. For the samples directly reduced at 700°C or 900°C (Figure 1J and K), the results were similar to those observed for samples that were calcined then reduced. Pure rutile phase was observed for samples reduced directly at 700°C or 900°C, with crystallite sizes of 39, and 44 nm, respectively.

A significant difference that is apparent in Figure 1 was observed in the x-ray diffraction rutile peak position for the 10Nb-TiO_2 when calcined and then reduced at 700 or 900°C compared to the rutile peak for TiO_2 reduced at 600°C (compare Figure 1G to E or F). A peak shift to lower 2-q value was observed for both the 10Nb-TiO_2 calcined then reduced and for the directly reduced samples. In order to observe whether the peak shift results from a change in the lattice caused by high temperature, pure TiO_2 was then calcined at 500°C followed by reduction at 700°C or 900°C. The TiO_2 sample reduced at 700°C (Figure 2A) had the rutile peak position at 2-q

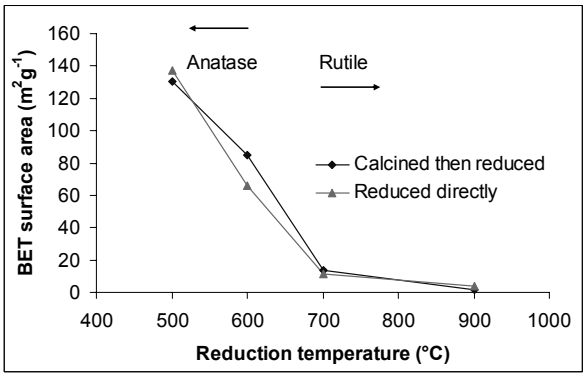

Figure 3. Plot of BET surface area vs. reduction temperature used to treat 10Nb-TiO_2.

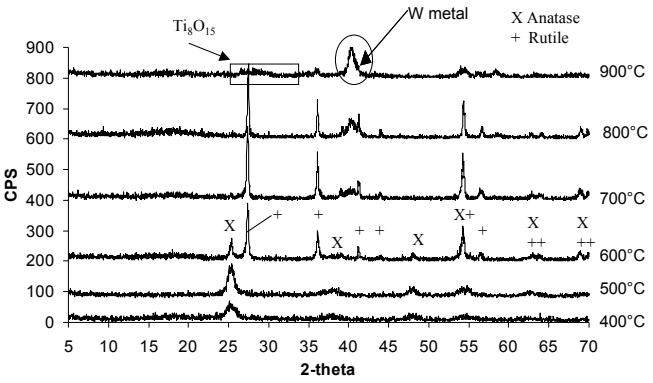

Figure 4. X-ray diffraction pattern of 10W-TiO_2 reduced at different temperatures.

27.495°, which is consistent with the reported value in the literature [01-089-4920]. However, the 10Nb-TiO_2 reduced at 700 or 900°C had the rutile peak shifted to lower 2-q at 27.268°, signifying an increase in the lattice constants. From the XRD pattern for TiO_2 reduced at 700°C, the crystallite size was calculated to be 49nm, whereas Nb doped titania formed smaller crystallites (39nm). The TiO_2 sample when reduced at 900°C (Figure 2B), however, produced a mixture of titanium suboxides Ti_6O_{11} and Ti_7O_{13}, which was not observed for the Nb doped titania samples. Niobium doping in this case prevents formation of titania sub-oxides, and the formation of a solid solution with Nb causes a lattice expansion.

In order to confirm that the peak shift was real and was not an artefact from the instrument, a standard was added to the samples. A small amount of sodalite standard for which the exact peak positions are known was added to the 10Nb-TiO_2 sample calcined and then reduced at 700°C. A shift to the lower 2-θ value was still observed in the XRD pattern. The rutile cell dimensions that are reported in the literature are a=b=4.584, c=2.953 [44]. The new cell dimensions for the sample calcined and then reduced at 700°C are a=b=4.626, c=2.964. The values reported for the treated samples were obtained by manually adjusting the cell parameters in the XRD-EVA program (Bruker). These values were found to be close to the ones calculated by modelling the diffraction pattern in the TOPAZ program (Bruker). The x-ray diffraction pattern for the 10Nb-TiO_2 sample calcined and then reduced at 700°C was analyzed with a modelling program, in order to determine the new lattice constants: a= b=4.62 and c=2.97, which were similar to those determined by the EVA program.

There is no observed peak shift for 10Nb-TiO_2 when reduced below 700°C. In order to observe the possibility of the presence of amorphous Nb, Nb(V) ethoxide was treated the same way as Nb-doped titania without the addition of any titanium propoxide. After drying, the XRD pattern exhibited the presence of amorphous material. After calcination at 500°C, the XRD pattern (not shown here) was of a single orthorhombic Nb_2O_5 phase. Since a separate phase of Nb_2O_5 was not observed for the Nb doped titania samples, it can be concluded that a solid solution of Nb doped titania was successfully synthesized in this study.

The BET surface area of the undoped titania calcined at 500°C was significantly lower (37.2 m^2g^{-1}) than that of the 10Nb-TiO_2 calcined at 500°C (150.4 m^2g^{-1}). The BET surface area decreased only slightly to 130.8 $m^2 g^{-1}$ when the 10Nb-TiO_2 sample was calcined and then reduced at 500°C. A sharp decrease in the surface area to 13.5 m^2g^{-1} with a transformation to the pure rutile phase was observed when the samples were reduced at 700°C. Unlike the sample calcined and then reduced at 600°C, the sample directly reduced at 600°C (Figure 1I) had a mixture of both anatase and rutile phase with a BET surface area of 65.7 m^2g^{-1}, which was lower than the 85.2 m^2g^{-1} surface area measured for the sample that was first calcined and then reduced at 600°C. Pure rutile phase was observed for samples reduced directly at 700°C or 900°C, with BET surface areas of 11.4 and 3.7 m^2g^{-1}, respectively. Figure 3 summarizes the BET data vs. the temperature used to treat the 10Nb-TiO_2 materials. As the treatment temperature increases, the BET surface area decreases, with the drop being most significant when the transformation from anatase to rutile occurs. The increasing crystallite size is consistent with the decrease in the BET surface area.

3.1.2. W-TiO_2

For the tungsten doped titania study, the tungsten dopant amount ranged from 5 to 20mol%. Figure 4 shows the XRD pattern for 10W-TiO_2 reduced at 400, 500, 600, 700, 800, or 900°C. Pure anatase is observed for samples reduced at 400 or 500°C, and a mixture of anatase and rutile is observed for samples reduced at 600°C. Tungsten segregation is observed when the material is reduced at temperatures higher than 600°C. A sub-stoichiometric titania peak (Ti_8O_{15}) is observed when the W doped titania is reduced at 900°C. The W doped titania behaves differently when reduced at temperatures higher than 600°C compared to the Nb doped titania. Niobium forms a solid solution in the rutile titania when reduced at 700 or 900°C, while tungsten does not form a single-phase solid solution in the titania lattice at those temperatures.

The phase identification results for Nb-TiO_2 and W-TiO_2 observed after heat treatments in reducing conditions show in some cases similar phases to those observed in oxidizing conditions in the TiO_2-WO_3 and TiO_2-Nb_2O_5 phase diagrams [45,46], while in some cases different phases were observed. Solubility limits of Nb_2O_5 in TiO_2 have been found to be approximately 6at.% for the rutile structure when calcined [8]. However, in the reducing condi-

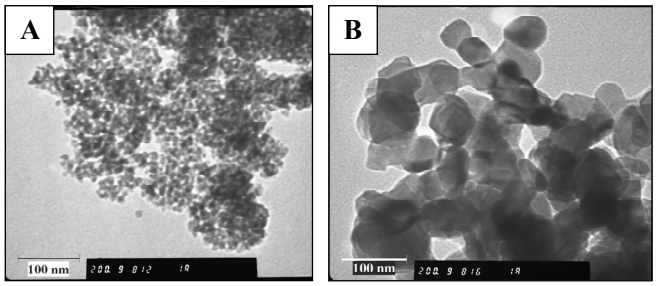

Anatase Rutile

Figure 5. TEM micrographs of A) 10Nb-TiO_2 calcined and then reduced at 500°C, B) 10Nb-TiO_2 calcined and then reduced at 700°C.

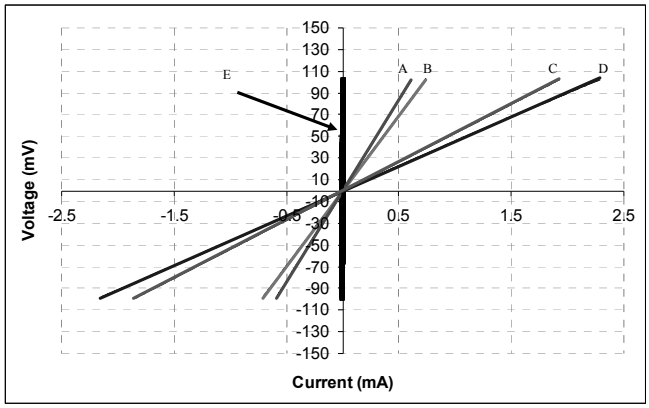

Figure 6. Voltage vs. current plots of 10Nb-TiO_2 and W-TiO_2. A) 10Nb-TiO_2 directly reduced at 700°C, B) 10Nb-TiO_2 calcined and then reduced at 700°C, C) 10Nb-TiO_2 calcined and then reduced at 900°C, D) 10Nb-TiO_2 directly reduced at 900°C, E) Anatase 10Nb-TiO_2 and all of W-TiO_2.

tions studied in this work, no new phase is detected up to concentrations of 30 mol% Nb. For the 10mol% Nb doped titania studied in this work, we only see the rutile TiO_2 phase when heating in reducing conditions, while Koninck et al. [8] observed the $TiNb_2O_7$ phase for 10mol% Nb-TiO_2 when calcining the material in air. The W-TiO_2 mixtures studied in this work formed single anatase phases and separate rutile and tungsten phases at different temperatures in reducing conditions, while WO_3 and TiO_2 do not form solid solutions when heated in air according to the phase diagram in [46].

Similarly to Nb-doped titania, the crystallite sizes for anatase W-TiO_2 increased as higher reducing temperatures were used. For example, the anatase crystallite size for 5W-TiO_2 grew to 29.2 nm when reduced at 600°C compared to 9.1 nm when the sample was reduced at 400°C. The XRD pattern for W doped titania with varying dopant amounts reduced at 400 or 500°C showed the presence of anatase titania, with the degree of crystallinity decreasing with increasing dopant amount (XRD pattern not shown here). The reason for the decrease of the crystallinity is not known. The BET surface area was found to increase with higher dopant amount. For example, a surface area of 83.6 m^2g^{-1} was observed for 5W-TiO_2 reduced at 500°C, and 119.8 m^2g^{-1} was observed for 20W-TiO_2. The BET surface area of Vulcan XC-72R is 200 m^2g^{-1}; since the density of W-TiO_2 and carbon are significantly different, the BET surface areas obtained in this study are comparable on a volumetric basis. The overall trends observed with the crystallite size decreasing as higher amounts of dopant were added correlate well with the increasing surface area as the dopant amount increased.

In order to observe the possibility of the presence of amorphous W, W(V) ethoxide was treated the same way as W-doped titania without the addition of any titanium propoxide. After drying, the XRD pattern exhibited presence of amorphous material. After calcination at 500°C, the XRD pattern showed the presence of monoclinic WO_3. Since a separate phase of WO_3 was not observed for the W doped titania samples, it can be concluded that a solid solution of W doped titania was successfully synthesized in this study. However, tungsten segregation was observed when the samples were reduced at temperatures greater than 600°C.

3.2. TEM/EDX characterization

TEM characterization was performed only on the 10Nb-TiO_2 samples. EDX was performed on three areas of the 10Nb-TiO_2 sample calcined at 500°C (anatase). The average atom% of Nb and Ti were found to be 11.2% (± 0.2%) and 88.8% (± 0.2%), respectively, which is close to the target composition of $Ti_{0.9}Nb_{0.1}O_2$.

The TEM micrograph of 10Nb-TiO_2 reduced at 500°C showed the presence of ~10-20 nm-sized fine anatase crystals (Figure 5A). The 10Nb-TiO_2 reduced at 700°C had 50-80 nm-sized rutile crystals (Figure 5B). The TEM results correlate well with both the XRD results and the BET surface area, where an increase in the crystallite size and a decrease in the surface area was observed with higher reduction temperatures. There is a significant difference in all the physical properties as the doped titania transforms from anatase to rutile phase.

3.3. Electrical Conductivity

The electrical conductivity of Nb-TiO_2 and W-TiO_2 was measured by pressing the material into pellets with no further heat-treatments. The goal was to measure the relative conductivity of materials treated under different temperatures in order to determine the conductivity of each phase. Therefore, the pellets were not sintered at high temperatures to consolidate them, as is usually performed when measuring the conductivity of powders, in order to avoid changing the phase to be measured. The electrical conductivity of both Nb-TiO_2 and W-TiO_2 pellets was measured using a DC technique. Since the density of both Nb-TiO_2 and W-TiO_2 were calculated, the volume of the pellets was kept similar in an attempt to equalize the effect of air gaps between particles for each material for better comparison. The thickness of the pellets was ~0.6 mm. Figure 6 shows the voltage versus current curves for these pellets.

The electrical resistance was determined from the slopes of the voltage vs. current curves, and both the resistance and the corresponding conductivity values are shown in Table 2 for 10Nb-TiO_2 and in Table 3 for W-TiO_2. The electrical resistances for anatase 10Nb-TiO_2 and all of the W-TiO_2 materials were extremely high. The conductivity of both the calcined and then reduced samples and of the directly reduced samples is similar. It should be mentioned that these conductivity values are not the absolute values for

Table 2. Resistance and conductivity values of 10Nb-TiO_2 treated under different temperatures.

Reduction T (°C)	Conductivity (μS cm^{-1}) of 10Nb-TiO_2	
	Calcined then reduced	Reduced directly
500	0.12	0.14
600	1.06	1.29
700	610	511
900	1400	1640

Table 3. Resistance and conductivity values of W-TiO_2 treated under different temperatures.

Reduction T (°C)	Conductivity (μS cm^{-1}) of W-TiO_2 reduced directly			
	5 W-TiO_2	10 W-TiO_2	15 W-TiO_2	20 W-TiO_2
400	0.01	0.07		0.04
500		1.42		
600	1.75		10.2	4.93

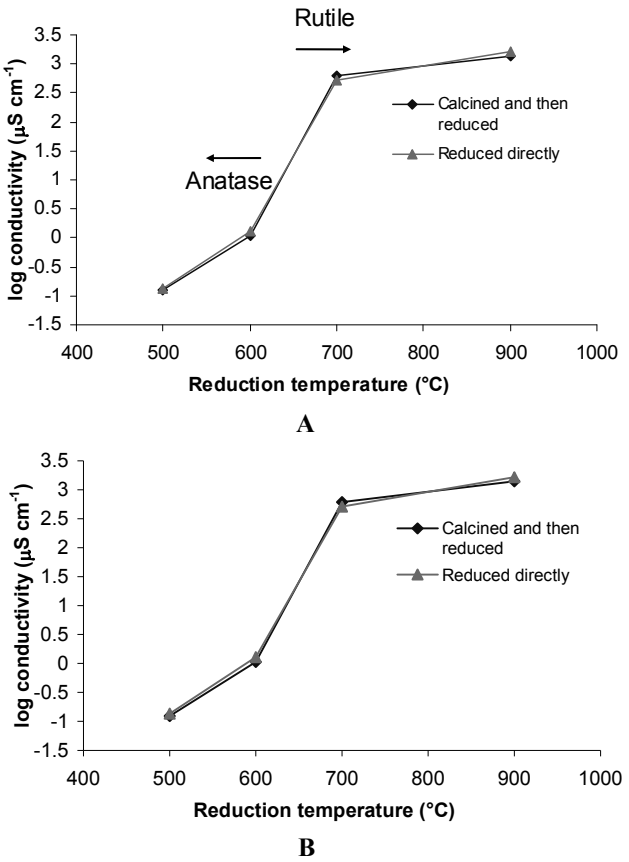

Figure 7. A) Conductivity vs. reduction temperature and B) conductivity vs. BET surface area plots of 10Nb-TiO_2 treated at different reduction temperatures.

these materials, since the pellets were not sintered to full density at high temperatures, and the porosity was not determined. The main intent was to observe any relative trends in conductivity between the materials while attempting to keep their porosity levels similar.

Figure 7 summarizes the conductivity versus temperature and

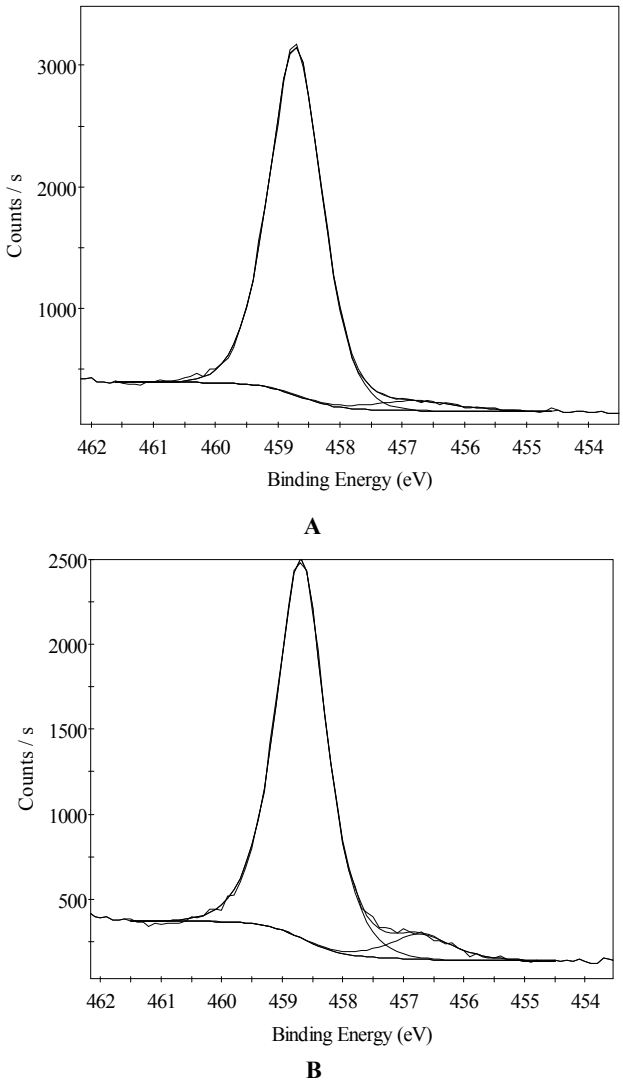

Figure 8. XPS spectrum of Ti $2p_{3/2}$ for A) 10 mol% Nb doped titania calcined at 500°C, B) 10mol%Nb doped titania calcined and then reduced at 700°C.

conductivity versus BET data for 10Nb-TiO_2, showing a significant increase in conductivity as 10Nb-TiO_2 transforms from anatase to rutile. Also the increase in conductivity with reduction temperature follows as inverse trend to that of the BET surface area. For 10Nb-TiO_2 to be used in a fuel cell, higher BET surface areas would be required, but it appears that for higher BET surface area the conductivity decreases significantly based on the processing conditions examined.

Since W-TiO_2 materials were extremely resistive when compared to 10Nb-TiO_2, no further tests were done on these materials.

3.4. XPS Analysis

XPS was used to determine the oxidation state of niobium and titanium in the doped oxides treated under different atmospheres. Figure 8 shows curve-fitted Ti $2p_{3/2}$ spectra of 10Nb-TiO_2 calcined at 500°C and 10Nb-TiO_2 calcined and then reduced at 700°C. Both

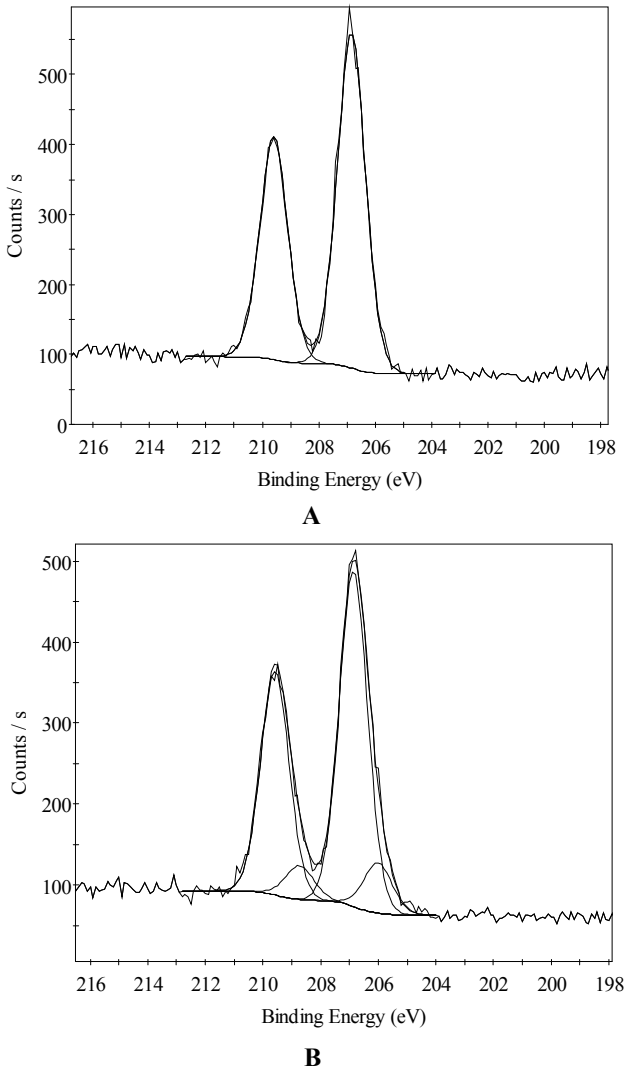

Figure 9. XPS spectrum of Nb 3d for a) 10mol% Nb doped titania calcined at 500°C, b) 10mol% Nb doped titania calcined and then reduced at 700°C.

spectra show Ti $2p_{3/2}$ peaks at 458.7 eV and 456.8 eV, which are consistent with Ti^{4+} and Ti^{3+}, respectively [8]. Most oxides are sub-stoichiometric in nature due to the defects in the crystal lattice, which may be why Ti^{3+} is present in the calcined sample. As the material is reduced, the peak at 456.8 eV increases significantly, which is indicative of the increase in the Ti^{3+} content.

Figure 9 shows curve-fitted Nb $3d_{5/2}$ and $3d_{3/2}$ spectra of the same samples. The Nb $3d_{5/2}$ peak at 206.9 eV for the calcined sample indicates the presence of Nb^{5+} alone. For the material calcined and then reduced at 700°C, an additional peak emerges at 206.0 eV, which is consistent with Nb^{4+} [8]. Nb^{4+} is absent for the calcined sample. Table 4 summarizes the observed trend. As the material is calcined at 500°C and then reduced at 700°C, there is an increase in the Ti^{3+} and Nb^{4+} concentrations. Since those cations act as electron donors, their presence significantly increases the electronic conductivity of the material. The XPS results provide an estimate of the charge carrier concentration, which is a factor in the conductivity. The other factor, mobility, depends on crystal phase and lattice and ionic size match. The overall conductivity of the structured material also depends on porosity and particle size.

Table 4. XPS ratio of Ti^{3+}/Ti^{4+} and Nb^{4+}/Nb^{5+} treated under different atmospheres and temperatures.

	Ti^{3+}/Ti^{4+}	Nb^{4+}/Nb^{5+}
10Nb-TiO_2 calcined at 500°C	0.04	0
10Nb-TiO_2 calcined and then reduced at 700°C	0.09	0.11

4. CONCLUSION

Niobium doped titania and tungsten doped titania were successfully fabricated by sol-gel techniques. Characterization of these materials was performed by XRD, BET, TEM, electrical conductivity, and XPS analysis of the doped materials prepared under different heat-treatment temperatures and partial oxygen pressures. The anatase to rutile transformation was observed when 10Nb-TiO_2 was reduced at temperatures higher than 600°C. In contrast with doped titania, the undoped titania formed sub-oxides when reduced at 900°C. In the XRD patterns, the rutile peaks shifted to lower 2θ values for the 10Nb-TiO_2 materials reduced at 700° or 900°C compared to the non-doped titania. The new lattice parameters were determined for these materials. The BET surface area decreased significantly for the rutile 10Nb-TiO_2 compared to the anatase. The rutile 10Nb-TiO_2 was the most conductive phase compared to the anatase 10Nb-TiO_2 and all of the W-TiO_2 samples, which were very resistive. Tungsten segregation was observed for the W-TiO_2 materials when these samples were reduced at temperatures greater than 600°C. The XPS analysis showed that in the materials studied, titanium is present in both the Ti^{3+} and Ti^{4+} states, and niobium exists in both the Nb^{4+} and Nb^{5+} states, with the proportion of Ti^{3+} and of Nb^{4+} increasing as higher processing temperatures are used. Based on the conductivity results, the rutile phase of 10Nb-TiO_2 was found to be a suitable candidate for PEMFC cathode catalyst supports. Further testing evaluating the stability of this support will be conducted.

REFERENCES

[1] C. Reiser, L. Bregoli, T. Patterson, J. Yi, J. Yang, M. Perry, T. Jarvi, Electrochemical and Solid-State Letters, 8, A273 (2005).
[2] M. Mathias, R. Makharia, H. Gasteiger, J. Conley, T. Fuller, C. Gittleman, S. Kocha, D. Miller, C. Mittesteadt, T. Xie, S. Yan, P. Yu, Interface, 14, 24 (2005).
[3]L. Roen, C. Paik, T. Jarvi, Electrochemical and Solid-State Letters, 7, A19 (2004).
[4] E. Antolini, Journal of Material Science, 38, 2995 (2003).
[5] B. Reddy, A. Khan, Catalysis Reviews, 47, 257 (2005).
[6] S. Tauster, S. Fung, R. Garten, Journal of the American Chemical Society 100, 170 (1978).
[7] F. Leroux, P. Dewar, M. Intissar, G. Ourard, L. Nazar, Journal of Materials Chemistry, 12, 3245 (2002).
[8] M. Koninck, P. Manseau, B. Marsan, Journal of Electroanalytical Chemistry, 611, 67 (2007).

[9] K. Park, K. Seol, Electrochemistry Communications, 9, 2256 (2007).
[10]G. Chen, S. Bare, T. Mallouk, Journal of the Electrochemical Society, 149, A1092 (2002).
[11]T. Ioroi, N. Fujiwara, S. Yamazaki, K. Yasuda, Electrochemistry Communications, 7, 183 (2005).
[12]T. Ioroi, H. Senoh, S. Yamazaki, Z. Siroma, N. Fujiwara, K. Yasuda, Journal of the Electrochemical Society, 155, B321 (2008).
[13]S. Padmanabhan, S. Pillai, J. Colreavy, S. Balakrishnan, T. Perova, Y. Gun'ko, S. Hinder, J. Kelly, Chemistry of Materials, 19, 4474 (2007).
[14]A. Ruiz, G. Dezanneau, J. Arbiol, A. Cornet, J. Morante, Chemistry of Materials, 16, 862 (2004).
[15]J. Arbiol, J. Carda, G. Dezanneau, A. Cirera, F. Peiro, A. Cornet, J. Morante, Journal of Applied Physics, 92, 853 (2002).
[16]D. Mulmi, T. Sekiya, N. Kamiya, S. Kurita, Y. Murakami, T. Kodaira, Journal of Physics and Chemistry of Solids, 65, 1181 (2004).
[17]E. Traversa, M. Di Vona, S. Licoccia, M. Sacerdoti, M. Carotta, M. Gallana, G. Martinelli, Journal of Sol-Gel Science and Technology, 19, 193 (2000).
[18]A. Ruiz, A. Calleja, F. Espiell, A. Cornet, J. Morante, Ieee Sensors Journal, 3, 189 (2003).
[19]A. Ruiz, G. Dezanneau, J. Arbiol, A. Cornet, J. Morante, Thin Solid Films 436, 90 (2003).
[20]A. Dros, D. Grosso, C. Boissiere, G. Soler-Lia, P. Albouy, H. Amenitsch, C. Sanchez, Microporous and Mesoporous Materials, 94, 208 (2006).
[21]E. Comini, M. Ferroni, V. Guidi, A. Vomiero, P. Merli, V. Mornadi, M. Sacerdoti, D. Mea, G. Sberveglieri, Sensors and Actutators B, 108, 21 (2005).
[22]S. Karvinen, Solid State Sciences, 5, 811 (2003).
[23]http://environmentalchemistry.com. 2008.
[24]H. Yang, D. Zhang, L. Wang, Materials Letters, 57, 674 (2002).
[25]S. Eibl, B. Gates, H. Knozinger, Langmuir, 17, 107 (2001).
[26]A. Rampaul, I. Parkin, S. O'Neill, J. DeSouza, A. Mills, N. Elliott, Polyhedron, 22, 35 (2003).
[27]X. Li, F. Li, C. Yang, W. Ge, Journal of Photochemistry and Photobiology A-Chemistry,141, 209 (2001).
[28]J. Haber, P. Nowak, Topics in Catalysis, 8, 199 (1999).
[29]D. Simakov, Y. Tsur, Journal of Nanoparticle Research, 10, 77 (2008).
[30]D. Morris, Y. Dou, J. Rebane, C. Michell, R. Edgell, D. Law, A. Vittadini, M. Casarin, Physical Review B, 61,13445 (2000).
[31]S. Park, S. Mho, E. Chi, Y. Kwon, H. Park, Thin Solid Films, 258, 5 (1995).
[32]B. Garcia, R. Fuentes, J. Weidner, Electrochemical and Solid-State Letters, 10, B108 (2007).
[33]H. Chhina, S. Campbell, O. Kesler, Journal of the Electrochemical Society, 156, B1232 (2009).
[34]H. Chhina, D. Susac, S. Campbell, O. Kesler, Electrochemical and Solid-State Letters, 12, B97 (2009).
[35]H. Lin, S. Kumon, H. Kozuka, T. Yoko, Thin Solid Films, 315, 266 (1998).
[36]I. Kartini, P. Meredith, J. Costa, G. Lu, Journal of Sol-Gel Science and Technology, 31, 185 (2004).
[37]R. Sharma, M. Bhatnagar, G. Sharma, Sensors and Actuators B, 46, 194 (1998).
[38]T. Anuradha, S. Ranganathan, Bull. Mater. Sci., 30, 263 (2007).
[39]H. Lin, H. Kozuka, T. Yoko, Journal of Sol-Gel Science and Technology, 19, 529 (2000).
[40]B. Cullity, Elements of X-Ray Diffraction, Addison Wesley Publishing Company, Inc. p. 1-30 (1978).
[41]S. Yin, R. Li, Q. He, T. Sato, Materials Chemistry and Physics, 75, 76 (2002).
[42]M. Mohammadi, M. Cordero-Cabrera, D. Fray, M. Ghorbani, Sensors and Actuators B, 120, 86 (2006).
[43]H. Hirashima, H. Imai, V. Balek, Journal of Non-Crystalline Solids, 285, 96 (2001).
[44]C. Legrand, J. Delville, Comptes Rendus Hebdomadaires des Séances de l'academie des Sciences 23, 944 (1953).
[45]T. Babich, A. Zagorodnyuk, G. Teterin, M. Khodus, P. Zhirnova, Zh. Neorg. Khim., 33, 996 (1988).
[46]L. Chang, M. Scroger, B. Phillips, J. Less-Common Met., 12, 51 (1967).